Editors' Suggestion | Featured in Physics

# Direct Observation of Sub-Poissonian Temporal Statistics in a Continuous Free-Electron Beam with Subpicosecond Resolution

S. Borrelli,* T. C. H. de Raadt, S. B. van der Geer, P. H. A. Mutsaers, K. A. H. van Leeuwen, and O. J. Luiten
*Department of Applied Physics, Eindhoven University of Technology, Groene Loper 19, 5612 AP, Eindhoven, The Netherlands*

(Received 25 August 2023; accepted 23 January 2024; published 15 March 2024)

We present a novel method to measure the arrival time statistics of continuous electron beams with subpicosecond resolution, based on the combination of an rf deflection cavity and fast single electron imaging. We observe Poissonian statistics within time bins from 100 to 2 ns and increasingly pronounced sub-Poissonian statistics as the time bin decreases from 2 ps to 340 fs. This 2D streak camera, in principle, enables femtosecond-level arrival time measurements, paving the way to observing Pauli blocking effects in electron beams and thus serving as an essential diagnostic tool toward degenerate electron beam sources for free-electron quantum optics.

DOI: 10.1103/PhysRevLett.132.115001

The concept of antibunched electron beams exhibiting sub-Poissonian statistics has emerged as a topic of great significance in electron microscopy and lithography, as well as in the rapidly expanding field of free-electron quantum optics. Sub-Poissonian electron beams hold immense potential as shot-noise-reduced probes for electron imaging with ultrahigh resolution and enhanced signal-to-noise ratio [1–3]. Furthermore, they are essential for establishing advanced quantum imaging techniques like ghost imaging and quantum holography [4–6]. Investigating the electron arrival time statistics and correlations plays a pivotal role in two aspects: understanding the fundamental behavior of free electrons and designing sub-Poissonian electron sources. The pioneering works of Kiesel *et al.* [7] and Kodama *et al.* [8] report the observation of anticorrelation between free electrons in coincidence experiments within time windows of 26 and 200 ps, respectively. More recently, Meier *et al.* [9] and Haindl *et al.* [10] observed the presence of strong energy anticorrelation between a few electrons confined in photoemitted pulses from nanometric needle tips. Furthermore, Keramati *et al.* [11] and Kuwahara *et al.* [12] demonstrated antibunching effects between electrons generated by, respectively, a photoemission gun and a spin-polarized source, in coincidence counting measurements with a resolution up to 48 ps. However, the direct observation of sub-Poissonian statistics in continuous electron beams within time windows of a few hundred femtoseconds has remained a challenging endeavor.



In this Letter, we present a novel method for quantifying the statistical properties of a continuous electron beam with subpicosecond resolution. We provide experimental results demonstrating the proposed technique's capability to continuously measure the electrons' concurrent arrival on a detector within time windows as short as a few hundred femtoseconds. These achievements are made possible through the unique combination of microwave-cavity-based electron beam deflection into a transverse Lissajous pattern followed by fast event-based electron imaging. Leveraging this combination, we have successfully developed a two-dimensional streak camera capable of subpicosecond resolution. To the best of our knowledge, the proposed method enabled for the first time the direct observation of sub-Poissonian statistics of a continuous electron beam across timescales ranging from picoseconds to hundreds of femtoseconds. Our finding revealed that, while electrons are randomly distributed according to Poisson statistics over time windows from 100 to 1 ns, the emergence of antibunching effects becomes apparent at picosecond timescales.

Measuring the electron arrival time statistics involves counting the number of electrons impinging on a detector within a given time window and determining the corresponding statistical distribution. One major limitation in such studies is the temporal resolution of the detector used to record electron events. Despite impressive progress, the achievable temporal resolution is still on the order of a few tens of picoseconds [13–17]. Before applying the proposed method to explore the subpicosecond timescale, we conducted benchmark studies to showcase the achievable results relying only on state-of-the-art detectors.

In the ultrafast transmission electron microscope (UTEM) at Eindhoven University of Technology (TU/e), we generated a 200 keV continuous electron beam at a current $I \sim 0.1$ nA and used a Timepix3 direct electron

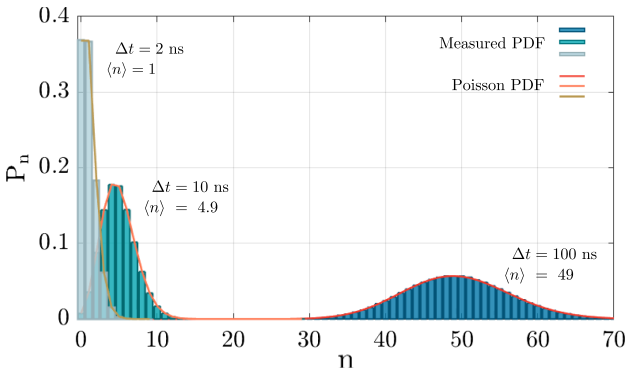


FIG. 1. Distribution of the simultaneous electron occurrences measured in $\Delta t = 100$, 10, 2 ns using the Timepix3 camera and the corresponding expected Poisson distribution. Total number of analyzed electron events is $\simeq 26 \times 10^6$ for $\Delta t = 100$, 10, 2 ns.

camera [18] to record electron events within a specific time window $\Delta t$. Figure 1 presents the probability distributions $P_n$ of the measured simultaneous occurrences of $n = 0, 1, \ldots$ electrons in the selected time bins $\Delta t = 100, 10, 2$ ns. Electron emission from a Schottky field emission gun can be modeled as a Poisson distribution, assuming a constant emission rate over time. The probability of $n$ electrons being emitted in $\Delta t$ is given by $P_n = [(\langle n \rangle^n e^{-\langle n \rangle})/n!]$, where $\langle n \rangle = (\langle I \rangle / e)\Delta t$. The solid curves in Fig. 1 represent the expected Poisson probability density function (PDF) for $\langle n \rangle$ equal to the average number of electrons we measured in each $\Delta t$. Clearly, the measured distributions are well described by a Poisson distribution, with a residual sum of squares on the order of $10^{-6}$ in all three cases.

The Timepix3 temporal resolution of 1.56 ns (per pixel) limits the study of the electron beam statistics to $\Delta t = 2$ ns at best. At shorter timescales, a loss of the random nature in the electron arrival time distribution may be observed due to the emergence of electron-electron anticorrelations. On one side, these correlations manifest the quantum-mechanical fermionic nature of electrons. According to the Pauli exclusion principle, the presence of an electron in a particular state inhibits the presence of another electron in the same state ("Pauli blockade"). Consequently, the probability of two or more electrons arrival within the coherence time of the beam is reduced, resulting in a sub-Poissonian distribution [12,19]. On the other side, the Coulomb repulsion between electrons emitted from the source's tip can also influence the dynamics and induce electron-electron anticorrelation within the characteristic time window of the interaction [11,20]. The method we propose here enables the investigation of timescales where the effects of Coulomb repulsion or the Pauli blockade become relevant in shaping the statistical distribution of electrons.

Figure 2(a) presents the layout of the TU/e rf-cavity-based UTEM [21]. This UTEM employs a commercial

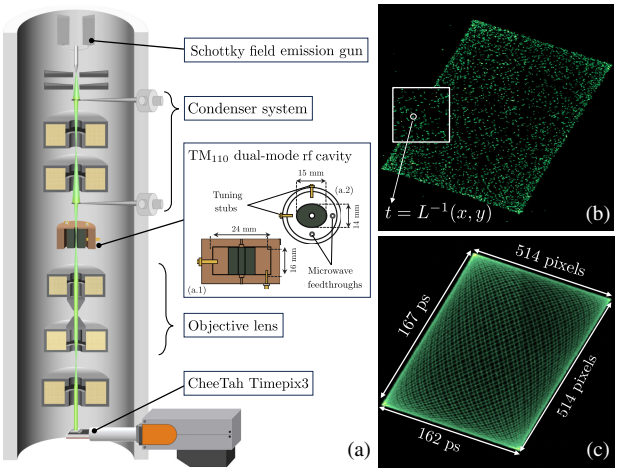


FIG. 2. (a) Illustration of the rf-cavity-based UTEM at TU/e. Inset: schematic representations include a (a.1) cut-through view and (a.2) top view of the rf cavity. (b) Lissajous pattern at $I = 0.1$ nA, imaged on the Timepix3 with 5 μs exposure. (c) Sum of 200 images.

200 keV FEI Tecnai TF20, generating a partially coherent continuous free-electron beam with 1 eV energy spread. The microscope is equipped with an rf cavity operated in $TM_{110}$ dual mode at resonance frequencies of 3.000 and 3.075 GHz, derived from the same 75 MHz driving signal [22]. The resulting electromagnetic field configuration induces a two-dimensional periodic deflection of the continuous electron beam into a transverse Lissajous pattern [see Fig. 2(c)] consistently generated at the same repetition rate as the driving signal, corresponding to a period of 13.3 ns. This pattern is detected using a Timepix3 direct electron camera mounted in the fluorescent screen chamber of the microscope [18]. This hybrid pixelated detector comprises a silicon sensor with an array of $514 \times 514$ pixel detectors. It allows for independent measurements of energy deposition (time over threshold, ToT) and timing information (time of arrival, ToA) of single electrons, as well as the determination of the position of the electron-activated pixels on the detector [23]. Upon striking the detector, an electron triggers the activation of a cluster of pixels featuring a given size, total ToT, and ToA values. Through a comprehensive characterization of the Timepix3 response to 200 keV single electrons, we determined the average number of pixels involved in a single electron hit (7 pixels) and the maximum variation in ToA values among the pixels within a cluster (30 ns). Additionally, we analyzed the distribution of the cumulative ToT across the pixels within a cluster and determined the average ToT of a single electron hit (7000 arbitrary units). This characterization enabled the development of a clustering algorithm that allowed us to reconstruct the timing and position of individual electrons incident on the detector from the activated cluster of pixels (see the Supplemental Material [24]).

Figure 2(b) shows a Lissajous pattern generated in the rf-cavity-based UTEM at $I = 0.1$ nA and imaged on the Timepix3 detector with 5 μs exposure. Each green dot in Fig. 2(b) represents a single electron that has landed on the detector at a specific time instant. The position of each electron dot is uniquely identified by the $(x, y)$ coordinate on the detector, assigned through the developed clustering algorithm. At the same time, the arrival time of each electron is recorded with nanosecond resolution. The Lissajous pattern's features are clearly recognizable in Fig. 2(c), which displays a composite pattern formed by all the electrons accumulated in 75000 Lissajous periods. Mathematically, this pattern is described by the vectorial function $L: t \mapsto (x, y)$ ("Lissajous function") defined as [24]

$$x(t) = A_1[\sin(\alpha_1 + K_1) - \sin(\alpha_1) - K_1\cos(\alpha_1)],$$
$$y(t) = A_2[\sin(\alpha_2 + K_2) - \sin(\alpha_2) - K_2\cos(\alpha_2)],$$

where $x(t)$ and $y(t)$ represent the transverse coordinates at the cavity exit of a generic electron in the beam along the horizontal and vertical axes of a Cartesian coordinate system. In these equations, $K_{1,2} \equiv [(L_{\mathrm{cav}}\omega_{1,2})/v_z]$ with $L_{\mathrm{cav}}$ being the cavity length, $\omega_1 = 2\pi \times 3.000$ and $\omega_2 = 2\pi \times 3.075$ GHz the two cavity's resonance frequencies, and $v_z$ the electron velocity; $\alpha_{1,2}(t) \equiv \omega_{1,2}t + \phi_{1,2}$ with $\phi_{1,2}$ denoting the phases of the cavity's fields at $t = 0$; $A_{1,2} \equiv +(-)(q_e v_z/m\gamma)(B_{1,2}/\omega_{1,2}^2)$ with $q_e$ being the electron charge and $\gamma$ the Lorentz factor. The amplitude factors $A_{1,2}$ measure the size of the $x$, $y$ side of the Lissajous pattern and depend on the rf power $W_{1,2} \propto B_{1,2}^2$ feeding the corresponding cavity mode. The phase difference between the two cavity modes $\phi_1 - \phi_2$ determines the spacing of the inner lines within the Lissajous figure.

One noteworthy characteristic of the Lissajous pattern is its time-dependent nature, associating a precise time instant with each position within the pattern. When considering a generic electron in a Timepix3-captured Lissajous pattern, the nanosecond-resolution ToA measurement provides information about the Lissajous period during which the electron landed on the detector within the exposure time. Additionally, the measured electron position $(x, y)$ within the pattern enables precise determination of its arrival time within the 13.3 ns Lissajous period. When imaging the entire Lissajous pattern across the $514 \times 514$ pixels of the detector, a maximum resolution of 315 fs/pixel can, in principle, be attained. However, enlarging the Lissajous figure using the microscope's imaging system allows for capturing only a fraction of the pattern corresponding to 1–2 ps. In this configuration, a resolution of a few femtoseconds per pixel can be achieved.

We employed this technique to study the arrival time statistics of a continuous free-electron beam generated in our UTEM at $I = 46.2$ nA. During the experiment, the beam was transversally deflected into a Lissajous pattern and imaged on the Timepix3, using the cavity's driving signal as a time stamp for the detector. For the data analysis, we utilized a fitting algorithm (see the Supplemental Material [24]) to fit the Lissajous function $L(t)$ to a measured pattern [see Figs. 3(a) and 3(b)]. To enhance our temporal resolution, we conducted a statistical analysis on the 1850 times magnified Lissajous pattern in Fig. 3(c), captured with an exposure time of 50 μs. The total beam current on the detector in this magnification mode is $I_{\mathrm{det}} = 0.12$ nA. This magnification yields a temporal resolution of approximately ~30 fs/pixel when other sources of uncertainty are neglected. A careful microscope alignment enabled magnifying around a central point without any rotation or shifting of the pattern. Consequently, the same Lissajous function evaluated in the best-fit parameters accurately describes the magnified pattern once enlarged by the same magnification factor. We increased the number of acquired events by continuously repeating the imaging process 1408 times, achieving a total exposure of 18.03 s.

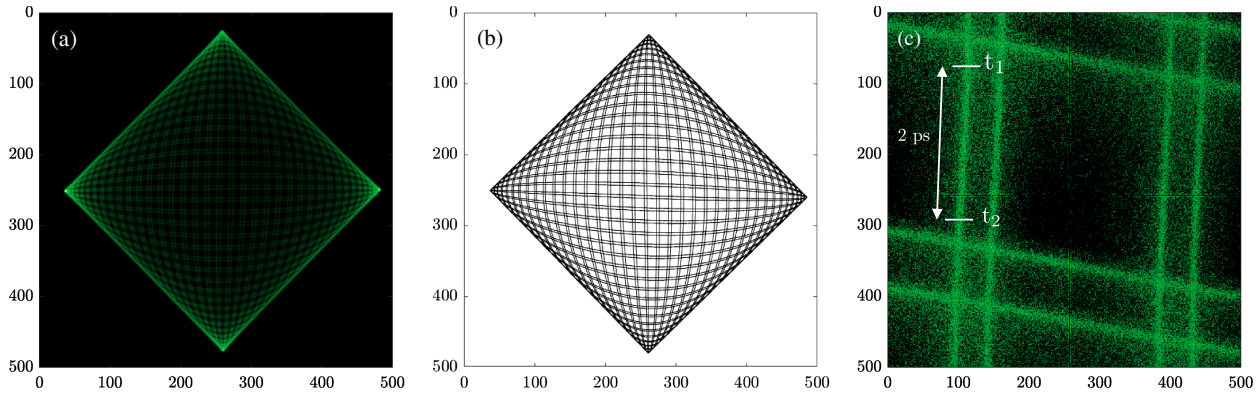


FIG. 3. (a) Composite image showing the sum of 1000 Lissajous patterns at $I = 0.1$ nA. (b) Lissajous function $L(t)$ fitted to the measured pattern [24]. (c) Composite image of six overlapped enlarged Lissajous patterns at $I = 46.2$ nA, each magnified 1850 times and captured using the Timepix3 detector with a 50 μs exposure.

To investigate the electron arrival time statistics, we selected the specific time bin $\Delta t$ defined by the line segment between the points $t_1$ and $t_2$ in Fig. 3(c). Given the measured coordinates of these two points, we determined the corresponding times within a Lissajous period through the inversion of the Lissajous function evaluated in the best-fit parameters. Accordingly, the selected line segment corresponds to $\Delta t = 2$ ps. In selecting the time bin, we excluded the crossing points between two inner lines and considered only the portion of the Lissajous pattern where the function is invertible [24]. In this case, for each electron event within the selected time bin, we could establish a Lissajous period based on the ToA measurement and determine the precise arrival time within the period by inverting the fitted Lissajous function. In practice, we tallied the number of electrons arriving at the detector within $\Delta t = 2$ ps for each measured Lissajous period. At later stages, we performed a more detailed analysis by partitioning the line segment between the points $t_1$ and $t_2$ in Fig. 3(c) into finer divisions of 1 ps, 500 fs, and 340 fs.

Figures 4(a)–4(d) present the measured probability $P_n$ of 0–5 simultaneous electron events in the selected time bins $\Delta t = 2$ ps, 1 ps, 500 fs, 340 fs, shown in purple bars. The orange bars represent the expected Poisson distribution $\tilde{P}_n = [(\langle n \rangle^n e^{-\langle n \rangle})/n!]$, with $\langle n \rangle$ equal to the measured average number of electrons in each $\Delta t$. The measured number of 0, 2, 3, 4, and 5 electron events is found to be smaller than expected from a Poisson distribution, while the number of single electron events is larger than predicted by a Poissonian behavior. These observed deviations are the signature of a sub-Poissonian distribution. The measured discrepancy is further evident in the plots in Figs. 4(e)–4(h), displaying for every $\Delta t$ the relative deviation of the measured distribution from the expected Poisson distribution, expressed as $1 - (\Delta P_n/\tilde{P}_n)$, with $\Delta P_n = P_n - \tilde{P}_n$. The displayed error bars, though challenging to discern, represent the statistical uncertainties associated with observing $N_n$ simultaneous $n$ electron events, computed as $\{[\sqrt{N_n(1-(N_n/N_{exp}))}]/\tilde{P}_n N_{exp}\}$, where $N_{exp}$ is the total number of measurements. Considering the measurements for $\Delta t = 2$ ps [Figs. 4(a) and 4(e)], we observe a reduction of 0.07%, 0.1%, 7%, 17%, and 26% in the number of 0, 2, 3, 4, and 5 electron events ($8 \times 10^8$, $1.1 \times 10^8$, $1.8 \times 10^7$, $2.1 \times 10^6$, $2.1 \times 10^6$, and $2.9 \times 10^5$), respectively. In comparison, the number of single electron events ($4.2 \times 10^8$) shows an increase of 2% compared to the expected Poisson distribution. The suppression of multiple electron events in favor of single electron events becomes even more pronounced when reducing the observation time window. Within the 340 fs time bin [Figs. 4(d) and 4(h)], the occurrences of 0 and 2 electron events ($7.4 \times 10^9$ and $2 \times 10^7$) drop by 0.2% and 28%, respectively. Meanwhile, the count of single electron events ($6.7 \times 10^8$) experiences a 3% increase. It should be noted that, as the time bin is reduced, the number of recorded events correspondingly decreases. Consequently, statistical errors for $n > 2$ can become too high to draw significant conclusions when examining very short timescales. For this reason, at 340 fs, we only present the data relative to the simultaneous arrival of 2 electrons on the detector, while at longer time windows, we can still contemplate 2, 3, and even 5 electron events. The dataset included in this study amounts to a total of $1.3 \times 10^9$ registered events.

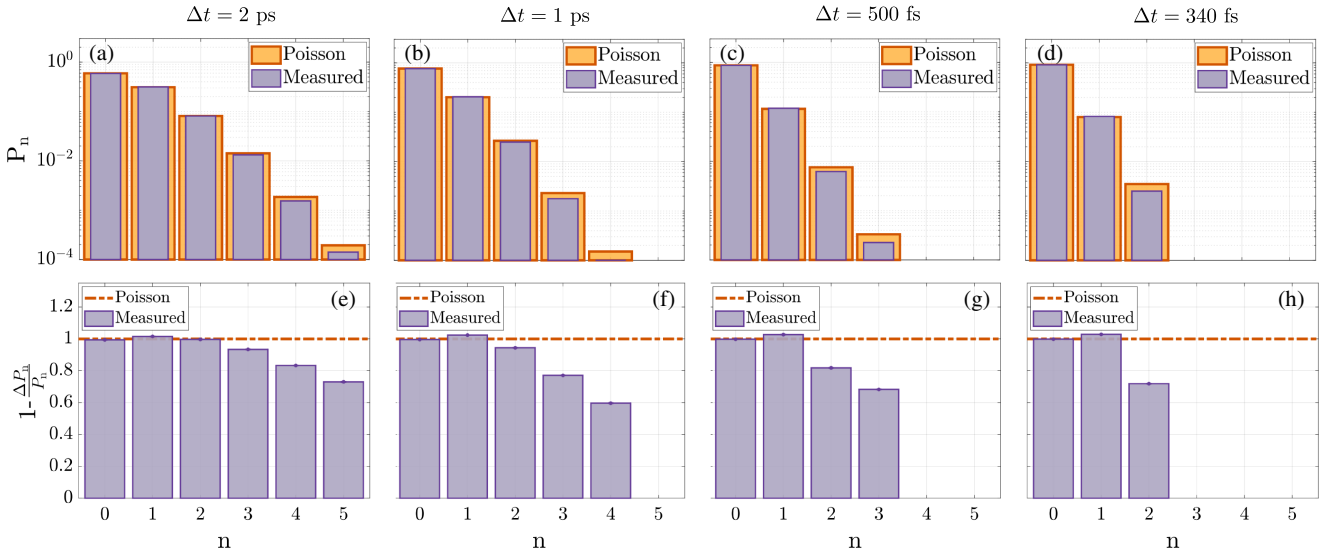


FIG. 4. (a)–(d) The distributions of the measured number of 0–5 simultaneous electron events, alongside the corresponding expected Poisson distributions with $\langle n \rangle =$ (a)0.52, (b) 0.26, (c) 0.13, (d) 0.09 for different time windows $\Delta t$. The corresponding deviations from the expected Poisson distribution are shown in (e)–(h). The dotted orange line represents the expectation for randomly distributed data according to a Poisson distribution.

We have measured arrival time statistics of continuous free-electron beams with ~300 fs resolution in a 200 keV UTEM. We find that the statistical distribution of electrons is Poissonian within time windows from 100 down to 1 ns, while we observe increasingly pronounced sub-Poissonian statistics as the counting time window decreases from 2 ps to 340 fs. The temporal resolution in the measurements was limited by the hit rate on the detector exceeding the maximum hit rate of the Timepix3 ($1.2 \times 10^8$ $s^{-1}$) at $I \sim$ few nA [24]. A higher resolution can be achieved by incorporating a fast beam blanker in the microscope column to reduce the effective hit rate on the detector.

Based on the current experimental results, it is challenging to ascertain unambiguously whether the observed antibunching is primarily caused by Coulomb repulsion among the electrons in the beam or quantum fermionic statistics. Properly discriminating between the two effects and establishing the corresponding timescales is an ongoing challenge [20]. Further experimental and theoretical investigations are thus necessary to explore the mechanism underlying the appearance of the two kinds of antibunching. However, Pauli blocking effects are expected to become significant only at subfemtosecond timescales for an unpolarized electron beam with an energy spread of 1 eV [24]. Additionally, we performed a classical charge particle tracing simulation of a 46.2 nA electron beam emission from a simplified yet realistic model of the Schottky field emission gun in our UTEM, incorporating all pairwise stochastic Coulomb interactions in the GPT code [25–27]. Preliminary results reveal that sub-Poissonian behavior becomes evident at a distance less than ~1 mm from the emission tip within time windows of 2 ps or shorter [24]. Achieving a higher temporal resolution makes it possible to delve into electron beam statistics on even shorter timescales. Furthermore, combining this advancement with a systematic study encompassing different electron beam extraction currents and possibly a spin-polarized electron source [12] would enable distinguishing Coulomb effects from Pauli blockade. While observing the Fermi-Dirac statistics holds significant importance from a fundamental physics perspective, gaining a deeper understanding of the dynamics underlying Coulomb repulsion between electrons in a beam is of great interest in free-electron quantum optics. These insights pave the way for the development of advanced techniques for electron beam manipulation and the realization of quantum electron sources for ultrahigh-resolution interaction-free electron imaging [28,29]. Furthermore, the method proposed and demonstrated in this study has the potential to shed light on the possible correlation between the arrival time statistics of electrons and radiation damage [30,31]. Finally, the versatility of the presented method extends its applicability beyond the specific case studied here, making it suitable for investigating and comparing the statistical properties of various electron sources.

O. L. conceived the original idea. S. B., T. R., P. M., K. L., and O. L. collectively designed the experimental setup, established the analysis procedure, and explored the theoretical framework. T. R. configured the Timepix3 detector for measurements and developed the data acquisition software. S. B. conducted preparatory simulations, analytically derived the fitting function, and prepared the microscope for the experiment. S. B. and T. R. jointly conducted the experiment, performed the data analysis, and generated the plots. S. B. and S. G. performed the simulative study in GPT. S. B. wrote the Letter, incorporating valuable inputs from all coauthors. This publication is part of the project *Dynamic Phase Space Shaping for Ultrafast Transmission Electron Microscopy* (DPSS, Project No. 741.018.302) of the research program ENW PPS-fonds (NWO-IPP), which is financed by the Dutch Research Council (NWO) and Thermo Fisher Scientific.

We are deeply grateful to Hein van den Heuvel and Harry van Doorn for their invaluable assistance in setting up the experiment and their prompt resolution of last-minute electronic challenges. Our heartfelt appreciation also goes to Stefan Kempers, Jim Franssen, and Erik Kieft for the enlightening discussions, constant support, and invaluable suggestions.

*s.borrelli@tue.nl

[1] M. I. Kolobov, *Quantum Imaging* (Springer Science & Business Media, New York, 2007).
[2] L. Mandel and E. Wolf, *Optical Coherence and Quantum Optics* (Cambridge University Press, Cambridge, England, 1995).
[3] O. S. Magaña-Loaiza and R. W. Boyd, Quantum imaging and information, Rep. Prog. Phys. **82**, 124401 (2019).
[4] T. B. Pittman, Y. H. Shih, D. V. Strekalov, and A. V. Sergienko, Optical imaging by means of two-photon quantum entanglement, Phys. Rev. A **52**, R3429 (1995).
[5] A. F. Abouraddy, B. E. Saleh, A. V. Sergienko, and M. C. Teich, Quantum holography, Opt. Express **9**, 498 (2001).
[6] B. Jack, J. Leach, J. Romero, S. Franke-Arnold, M. Ritsch-Marte, S. M. Barnett, and M. J. Padgett, Holographic ghost imaging and the violation of a Bell inequality, Phys. Rev. Lett. **103**, 083602 (2009).
[7] H. Kiesel, A. Renz, and F. Hasselbach, Observation of Hanbury Brown–Twiss anticorrelations for free electrons, Nature (London) **418**, 392 (2002).
[8] T. Kodama, N. Osakabe, and A. Tonomura, Correlation in a coherent electron beam, Phys. Rev. A **83**, 063616 (2011).
[9] S. Meier, J. Heimerl, and P. Hommelhoff, Few-electron correlations after ultrafast photoemission from nanometric needle tips, Nat. Phys. **19**, 1402 (2023).
[10] R. Haindl, A. Feist, T. Domröse, M. Möller, J. H. Gaida, S. V. Yalunin, and C. Ropers, Coulomb-correlated electron number states in a transmission electron microscope beam, Nat. Phys. **19**, 1417 (2023).

[11] S. Keramati, W. Brunner, T. J. Gay, and H. Batelaan, Non-Poissonian ultrashort nanoscale electron pulses, Phys. Rev. Lett. **127**, 180602 (2021).
[12] M. Kuwahara, Y. Yoshida, W. Nagata, K. Nakakura, M. Furui, T. Ishida, K. Saitoh, T. Ujihara, and N. Tanaka, Intensity interference in a coherent spin-polarized electron beam, Phys. Rev. Lett. **126**, 125501 (2021).
[13] T. Gys, Micro-channel plates and vacuum detectors, Nucl. Instrum. Methods Phys. Res., Sect. A **787**, 254 (2015).
[14] A. Tremsin, J. Vallerga, and O. Siegmund, Overview of spatial and timing resolution of event counting detectors with microchannel plates, Nucl. Instrum. Methods Phys. Res., Sect. A **949**, 162768 (2020).
[15] F. Carnesecchi, Performance of the ALICE time-of-flight detector at the LHC, J. Instrum. **14**, C06023 (2019).
[16] F. Powolny, E. Auffray, S. Brunner, E. Garutti, M. Goettlich, H. Hillemanns, P. Jarron, P. Lecoq, T. Meyer, H. Schultz-Coulon *et al.*, Time-based readout of a silicon photomultiplier (SiPM) for time of flight positron emission tomography (TOF-PET), IEEE Trans. Nucl. Sci. **58**, 597 (2011).
[17] S. Kempers, S. Borrelli, E. Kieft, H. van Doorn, P. Mutsaers, and O. Luiten, Photodiode-based time zero determination for ultrafast electron microscopy, Struct. Dyn. **10**, 064301 (2023).
[18] Amsterdam Scientific Instruments (ASI), https://www.amscins.com/product/cheetah/.
[19] M. Silverman, On the feasibility of observing electron antibunching in a field-emission beam, Phys. Lett. **120A**, 442 (1987).
[20] T. Kodama and N. Osakabe, Mechanism for correlation in a coherent electron beam, Microscopy **68**, 133 (2019).
[21] S. Borrelli, S. T. Kempers, P. H. Mutsaers, and O. J. Luiten, in *Structural Dynamics with X-ray and Electron Scattering*, edited by K. Amini, A. Rouzée, and M. J. J. Vrakking (Royal Society of Chemistry, Cambridge, 2023), Vol. 25, pp. 557–588, 10.1039/BK9781837671564-00557.
[22] J. Van Rens, W. Verhoeven, E. Kieft, P. Mutsaers, and O. Luiten, Dual mode microwave deflection cavities for ultrafast electron microscopy, Appl. Phys. Lett. **113**, 163104 (2018).
[23] T. Poikela, J. Plosila, T. Westerlund, M. Campbell, M. De Gaspari, X. Llopart, V. Gromov, R. Kluit, M. Van Beuzekom, F. Zappon *et al.*, Timepix3: A 65k channel hybrid pixel readout chip with simultaneous toa/tot and sparse readout, J. Instrum. **9**, C05013 (2014).
[24] See Supplemental Material at http://link.aps.org/supplemental/10.1103/PhysRevLett.132.115001 for detailed information on the developed clustering algorithm for reconstructing single electron events in a Timepix3 measurement; the microwave-cavity-based deflection of the electron beam into a Lissajous pattern and its mathematical description; the data analysis strategy employed; the beam coherence analysis; and the simulative study of electron emission from a Schottky field emission gun in the General Particle Tracer code.
[25] S. B. van der Geer and M. J. de Loos, Pulsar physics and the general particle tracer (GPT) code, http://www.pulsar.nl/gpt.
[26] S. van der Geer, O. Luiten, M. de Loos, G. Pöplau, and U. van Rienen, 3D space-charge model for GPT simulations of high brightness electron bunches, in *Journal of Physics: Conference Series*, Vol. 175 (Institute of Physics Publishing, Bristol, 2005), p. 101.
[27] G. Poplau, U. van Rienen, B. van der Geer, and M. de Loos, Multigrid algorithms for the fast calculation of space-charge effects in accelerator design, IEEE Trans. Magn. **40**, 714 (2004).
[28] P. Kruit, R. G. Hobbs, C.-S. Kim, Y. Yang, V. R. Manfrinato, J. Hammer, S. Thomas, P. Weber, B. Klopfer, C. Kohstall *et al.*, Designs for a quantum electron microscope, Ultramicroscopy **164**, 31 (2016).
[29] P. Bøggild, J. M. Caridad, C. Stampfer, G. Calogero, N. R. Papior, and M. Brandbyge, A two-dimensional Dirac fermion microscope, Nat. Commun. **8**, 15783 (2017).
[30] E. J. VandenBussche and D. J. Flannigan, Reducing radiation damage in soft matter with femtosecond-timed single-electron packets, Nano Lett. **19**, 6687 (2019).
[31] C. Kisielowski, P. Specht, B. Freitag, E. R. Kieft, W. Verhoeven, J. F. van Rens, P. Mutsaers, J. Luiten, S. Rozeveld, J. Kang *et al.*, Discovering hidden material properties of $MgCl_2$ at atomic resolution with structured temporal electron illumination of picosecond time resolution, Adv. Funct. Mater. **29**, 1807818 (2019).